Journal of Materials Science & Technology 35 (2019) 369–373

Contents lists available at ScienceDirect

Journal of Materials Science & Technology

journal homepage: www.jmst.org

Research Article

A promising new class of irradiation tolerant materials: $Ti_2ZrHfV_{0.5}Mo_{0.2}$ high-entropy alloy

Yiping Lu[a,1], Hefei Huang[b,*,1], Xuzhou Gao[c,1], Cuilan Ren[b], Jie Gao[b], Huanzhi Zhang[a], Shijian Zheng[d,*], Qianqian Jin[d], Yonghao Zhao[c,*], Chenyang Lu[e], Tongmin Wang[a,*], Tingju Li[a]

[a] Key Laboratory of Solidification Control and Digital Preparation Technology (Liaoning Province), School of Materials Science and Engineering, Dalian University of Technology, Dalian 116024, China
[b] Shanghai Institute of Applied Physics, Chinese Academy of Sciences (CAS), Shanghai 201800, China
[c] School of Materials Science and Engineering, Nanjing University of Science and Technology, Nanjing 210094, China
[d] Shenyang National Laboratory for Materials Science, Institute of Metal Research, Chinese Academy of Sciences, Shenyang 110016, China
[e] Department of Nuclear Engineering and Radiological Sciences, University of Michigan, Ann Arbor, MI 48109-2104, USA

ARTICLE INFO

Article history:
Received 28 August 2018
Received in revised form
10 September 2018
Accepted 11 September 2018
Available online 21 September 2018

Keywords:
High-entropy alloy
Irradiation resistance
Microstructural characterization
Defects evolution

ABSTRACT

Recently, high-entropy alloys (HEAs) or multi-principal-element alloys with unprecedented physical, chemical, and mechanical properties, have been considered as candidate materials used in advanced reactors due to their promising irradiation resistant behavior. Here, we report a new single-phase body-centered cubic (BCC) structured $Ti_2ZrHfV_{0.5}Mo_{0.2}$ HEA possessing excellent irradiation resistance, i.e., scarcely irradiation hardening and abnormal lattice constant reduction after helium-ion irradiation, which is completely different from conventional alloys. This is the first time to report the abnormal XRD phenomenon of metallic alloys and almost no hardening after irradiation. These excellent properties make it to be a potential candidate material used as core components in next-generation nuclear reactors. The particular irradiation tolerance derives from high density lattice vacancies/defects.

1. Introduction

Nuclear energy, due to cleanness, economy and reliability, is the world's 3rd largest energy after thermal power and hydropower. Structure materials used in nuclear power plant are generally required to have comprehensive properties such as excellent high-temperature properties, irradiation and corrosion resistances [1,2]. For the fuel cladding material used in nuclear reactors, its irradiation-resistant properties are of significant importance because the large doses of neutron irradiation result in vacancy, dislocation and solute precipitation as well as H and He transmutation gas damage which further result in swelling, hollow, material embrittlement and hardening as well as failure in service [1–6]. Currently, the nuclear fuel rods are made by Zr alloys. However, Zr alloys react with water at high temperature to generate hydrogen, which can cause serious hydrogen explosion such as the accident in Fukushima [7].

With continuously improved requirements for the service life, safety and economy of the next generation of the nuclear power, the demanding for the comprehensive properties of the structure materials are becoming unprecedentedly critical, especially for the fuel cladding materials. Recent investigations indicate that oxide dispersion strengthened (ODS) steels and SiC ceramic seem to be the ideal candidate materials for the next generation of nuclear structure materials [7–11]. However, large-scale preparation of the ODS steels with uniform microstructures for industrial applications is extremely difficult. The welding properties of SiC ceramic are poor, which also limits the application in nuclear power plants. Nanomaterials, such as nanocrystalline materials, multilayered nanomaterials, and nanofoams, are numerously investigated and shown excellent irradiation-tolerant properties [12–15]. However, nano-materials with the high volume fractions of surface or interface are thermodynamically unstable, which are unreliable for long operational time at high temperatures [12,16].

Recently, high-entropy alloys (HEAs) or multi-principal-element alloys, as a new type of alloys, are becoming new research

* Corresponding authors.
E-mail addresses: huanghefei@sinap.ac.cn (H. Huang), sjzheng@imr.ac.cn (S. Zheng), yhzhao@njust.edu.cn (Y. Zhao), tmwang@dlut.edu.cn (T. Wang).
[1] These authors contributed equally to this work.

https://doi.org/10.1016/j.jmst.2018.09.034
1005-0302/

frontier in the metallic materials community [17–21]. Compared to the conventional alloys with one or two major elements, HEAs generally contain 5–13 principal elements with the concentrations of each element between 5 and 35 at.% [19]. The latest researches indicate that some HEAs exhibit better irradiation resistance than traditional alloys, such as enhanced swelling resistance, reduced dislocation evolution, significant reduction in damage accumulation and so on [16,22–25]. Therefore, the HEAs became promising candidates satisfying the critical requirements of complex environments which integrated high temperatures, corrosive and extreme irradiation exposures together.

Nevertheless, literature-reported irradiation-resistant HEAs are limited to those with equal molar ratio and single face-centered cubic (FCC) structure [26]. The irradiation behavior of non-equal molar ratio body-centered cubic (BCC) structured HEAs has not been investigated yet.

Here, we designed irradiation-resistant BCC HEA which can meet the requirements of the next generation nuclear power plant. We selected Ti element due to its good corrosion resistance, Mo and V elements due to their good high temperature performance, and Hf and Zr elements due to their good neutrons-penetrating properties.

2. Experiment procedures

The $Ti_2ZrHfV_{0.5}Mo_{0.2}$ HEAs were prepared by vacuum arc melting in Ti-gettered high-purity argon atmosphere with constituent elemental purity higher than 99.95 wt%. Based on the model reported by Guo et al. where BCC structure of HEAs can be obtained when the valence electron concentration (VEC) < 6.87 [27], we design a single BCC-structured non-equal molar ratio $Ti_2ZrHfV_{0.5}Mo_{0.2}$ HEA with the VEC value of 4.404 which displays excellent ductility and strength (Fig. S1). Moreover, to achieve a homogeneous distribution of elements, each alloy was remelted and flipped five times with electromagnetic stirring. The prepared button-shaped specimens were approximately 30 mm in diameter and 15 mm in thickness. The details of the melting process can be found in Ref. [28]. The grain size of the cast $Ti_2ZrHfV_{0.5}Mo_{0.2}$ HEA is about 300–500 μm, as revealed by the scanning electron microscopy (SEM) image shown in Fig. S2(a). Elemental mapping in Fig. S2(b–d) indicates that the elemental distribution of $Ti_2ZrHfV_{0.5}Mo_{0.2}$ alloy is uniform without elemental segregation, inhomogeneity or precipitation.

In this work, ion beam irradiation has been conducted on $Ti_2ZrHfV_{0.5}Mo_{0.2}$ HEA to study its irradiation behavior. The $Ti_2ZrHfV_{0.5}Mo_{0.2}$ HEA alloys were irradiated with 3 MeV He^+ ions to high dose at 600 °C. Then the irradiated alloys were analyzed by X-ray diffraction (XRD), transmission electron microscopy (TEM), nanoindenter and positron annihilation spectroscopy (PAS).

The samples used in this study were taken from the as-cast ingots. Bulk $Ti_2ZrHfV_{0.5}Mo_{0.2}$ HEA sample were first cut into 1 mm thick sheets (10 mm × 6.5 mm) then mechanical polished with silicon carbide paper and diamond polishing paste. These sheets were subsequently prepared by electro-polishing at 36 V for about 10 s in an aqueous solution of 50% H_2SO_4 and 40% glycerin below 0 °C, followed by ultrasonic cleaning with acetone, absolute ethyl alcohol and deionized water sequentially. The prepared samples were irradiated at 600 °C with 3 MeV He^+ ions to the dosages of 5×10^{15}, 1×10^{16} and 3×10^{16} ions/cm^2 using a 4 MV Pelletron accelerator located at the Shanghai Institute of Applied Physics, Chinese Academy of Sciences (SINAP-CAS). The damage profiles were calculated using the Stopping and Range of Ions in Matter (SRIM) 2008 (Fig. S3) [29]. The displacement energy for the elements of Ti, Cr, Hf, V, Mo is 30, 40, 90, 40, 60 eV, respectively. Note that the calculations were achieved with "K-P quick calculation", and the dpa were obtained using the vacancy.txt file [30].

The lattice structure of unirradiated and irradiated samples was characterized using a Bruker D8 XRD equipped with Cu K_{a1} radiation source (λ = 1.5406 Å) operating at 40 kV and 40 mA, with a 2θ range of 10°–90°. Additionally, the ion irradiation-induced microstructural evolution of irradiated $Ti_2ZrHfV_{0.5}Mo_{0.2}$ HEA samples was characterized using a FEI-Tecnai G^2 20 S-TWIN transmission electron microscope operated at 200 kV. Furthermore, the G200 nanoindenter was also used in this study to measure the nanohardness of all investigated samples. A diamond Berkovich tip (model TB13989-XP) with a radius of 20 nm was employed. The experimental hardness was determined by analyzing the load-displacement (P-h) curves using the Oliver and Pharr method [31]. Additionally, the positron annihilation experiments were performed at room temperature using an energy-variable slow positron beam facility. Positrons were generated by a ^{22}Na irradiation source, and then moderated by tungsten. Beam energy was changed from 0.25 to 20 keV during Doppler Broadening Energy Spectroscopy (DBES) measurement [32]. Two parameters, namely *S* and *W* parameters respectively, were introduced in the analysis of the spectra. The mean implantation depth *Z*(*E*) of the positron is defined by the incident energy and calculated by the following equation [33]:

$$Z(E) = (40/\rho)\cdot E^{1.6} \quad (1)$$

where *Z*(*E*) is expressed in the units of nanometer, *q* is the density of the specimen with the units of g/cm^3 and *E* is the incident positron energy in keV.

3. Results and discussion

3.1. XRD analysis

The XRD patterns of the raw and irradiated $Ti_2ZrHfV_{0.5}Mo_{0.2}$ HEA are shown in Fig. 1(a). It is clearly shown that the $Ti_2ZrHfV_{0.5}Mo_{0.2}$ HEA is a BCC single phase. After irradiation, the diffraction peaks of $Ti_2ZrHfV_{0.5}Mo_{0.2}$ HEA shift gradually towards the bigger 2θ values, implying a decrease of lattice parameter. As shown in Fig. 1(a, b), the lattice parameter of the initial HEA is 3.4584 nm, and it is decreased by 0.676% to 3.4350 nm after irradiation dose of 3×10^{16} ions/cm^2. The observed irradiation-caused shrink of lattice parameter in our HEA is different from the conventional alloys, such as 316L, 304H and Zr-Nb alloys of which the lattice parameter expands after irradiation [34,35]. To our knowledge, this is the first time to report the abnormal XRD phenomenon of metallic alloys and almost no hardening after irradiation. The extreme lattice distortion exists in the HEA due to different atomic sizes of the solutes, and the irradiation relaxes the lattice distortion resulting in the lattice shrink. In contrast, the irradiation induced lattice distortion into the equilibrium lattice of the conventional alloys, resulting in a lattice expansion.

3.2. TEM characterization

Fig. 2(a) shows the bright-field TEM micrographs of the FIB prepared He-ion irradiated sample at an ion dose of 3×10^{16} ions/cm^2. The TEM analysis was conducted in three regions (Regions b–d in Fig. 2), each with different depths from the surface. According to the damage profile calculated using Stopping and Range of Ions in Matter (SRIM) 2008, as shown in Fig. S3, three regions at different locations along the penetration track were selected to investigate the ion irradiation induced microstructural changes, as shown in Fig. 2(e–g). The helium bubbles distributes in a narrow region with a width of about 1–1.5 μm. With increasing irradiation dose, the maximum density of helium bubbles occurs at

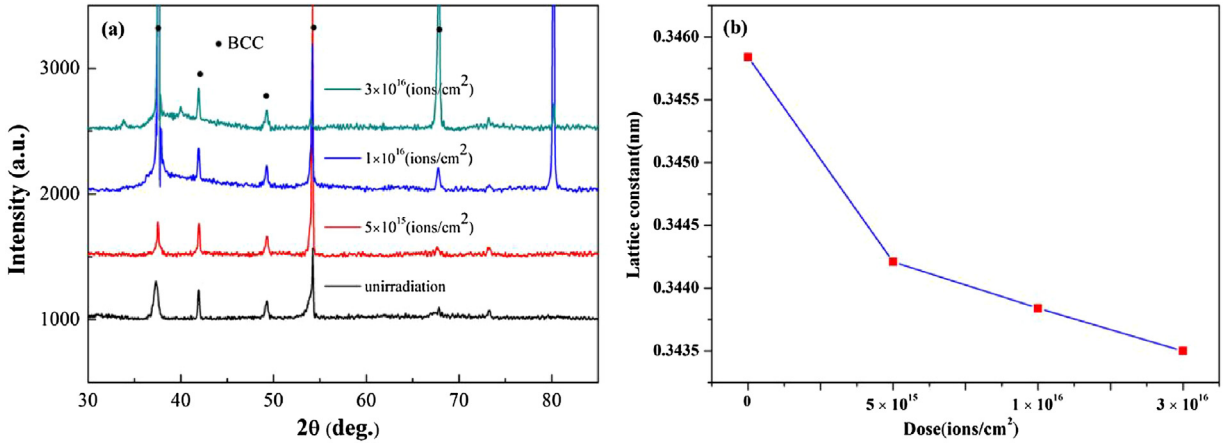

Fig. 1. (a) XRD patterns of initial and irradiated $Ti_2ZrHfV_{0.5}Mo_{0.2}$ HEA at ion doses of 5×10^{15}, 1×10^{16} and 3×10^{16} ions/cm^2, respectively. (b) Variation of lattice parameter versus irradiation doses.

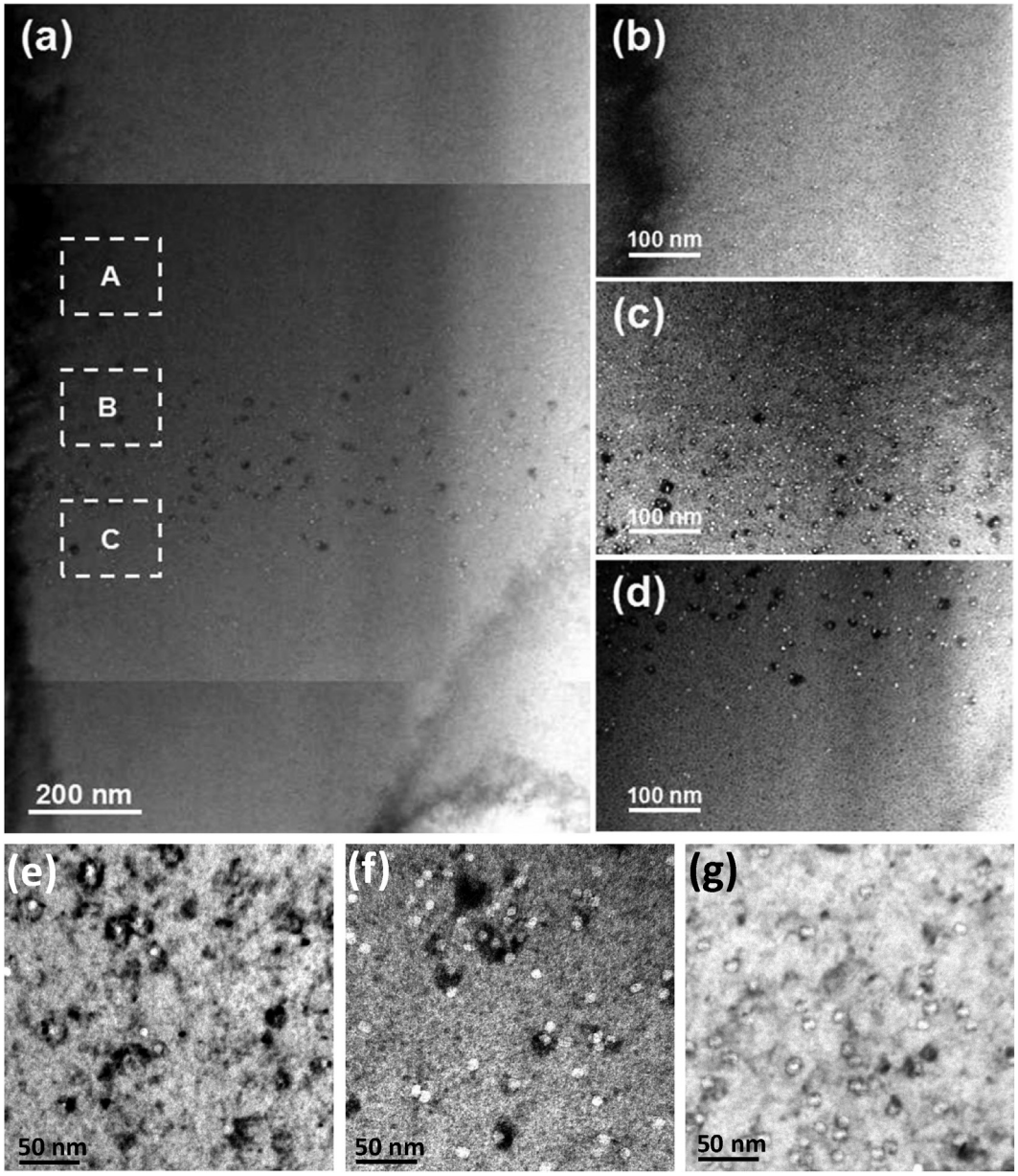

Fig. 2. (a) TEM images of $Ti_2ZrHfV_{0.5}Mo_{0.2}$ HEA at irradiation dose of 3×10^{16} ions/cm^2. The maximum density of He bubbles appears at 7.3 μm from the surface. (b–d) Magnified images of regions "A" "B" and "C" in (a) respectively. (e–g) Magnified images at peak damage region of the irradiated samples with ion dose of respectively 5×10^{15}, 1×10^{16} and 3×10^{16} ions/cm^2.

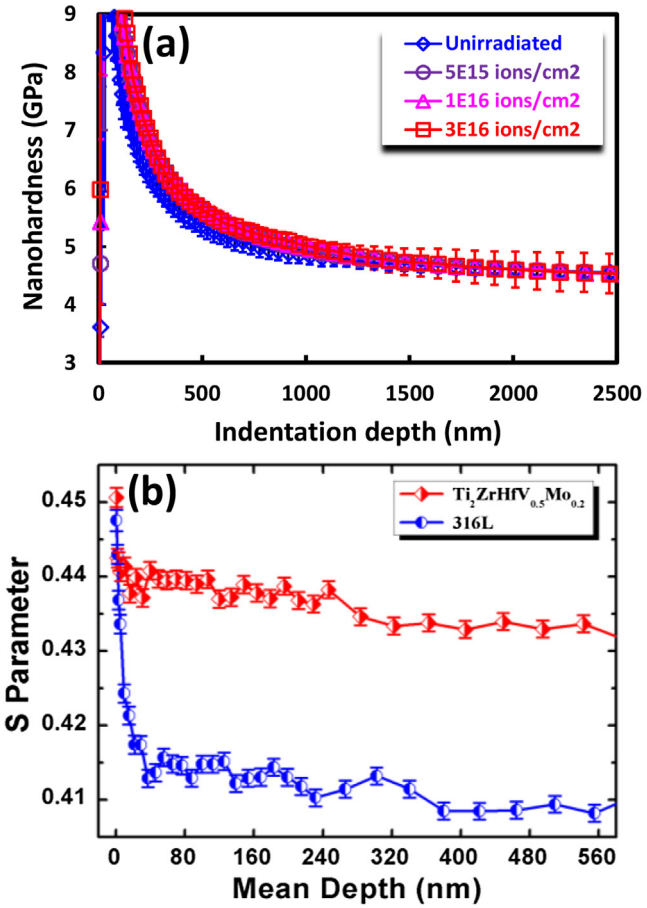

Fig. 3. (a) Average nanoindentation hardness versus the indentation depth of unirraidated and irradiated $Ti_2ZrHfV_{0.5}Mo_{0.2}$ HEA at ion doses of 5×10^{15}, 1×10^{16} and 3×10^{16} ions/cm^2, respectively. (b) Positron annihilation experiment of $Ti_2ZrHfV_{0.5}Mo_{0.2}$ HEA and 316L steel.

6 μm (5×10^{15} ions/cm^2), 7 μm (1×10^{16} ions/cm^2) and 7.3 μm (3×10^{16} ions/cm^2) from the surface to inner of $Ti_2ZrHfV_{0.5}Mo_{0.2}$ HEA, respectively, as shown in Fig. 2(e–g). The sizes of helium bubbles (~4–7 nm) were similar to that observed in nickel and Ni-SiC_{NP} material irradiated on the same condition [34]. However, the number density of helium bubbles in all the irradiated samples was estimated to range from 3.4 to 11.9×10^{21} m^{-3}, which is one order of magnitude lower than the values ($(4–14)\times10^{22}$ m^{-3}) reported by the reference [36].

3.3. Nanoindentation measurement

To further study performance variation of the $Ti_2ZrHfV_{0.5}Mo_{0.2}$ HEA after irradiation, the nanoindentation hardness of unirraidated and irradiated $Ti_2ZrHfV_{0.5}Mo_{0.2}$ HEA samples was measured. In this study, eight single indents were made for each sample in order to ensure the accuracy of the experimental results. The average nanoindentation hardness of all the investigated samples was plotted as a function of the indentation depth, as shown in Fig. 3(a). It is pleasantly surprised that the average nanoindentation hardness of irradiated $Ti_2ZrHfV_{0.5}Mo_{0.2}$ HEA samples kept almost the same as the unirradiated one. As we all know, hardening is common in conventional alloys after irradiation but the single-BCC structured $Ti_2ZrHfV_{0.5}Mo_{0.2}$ HEA exhibits an encouraging feature that is almost no hardening. The particular characteristic of $Ti_2ZrHfV_{0.5}Mo_{0.2}$ HEA will hopefully/greatly improve the life of the nuclear structural material so that can significant improve the security and economy of nuclear power station.

The irradiation induced embrittlement is one of the main failure modes of structural materials for nuclear power plant, especially for the reactor vessel [37]. It is generally accepted that the formation of intergranular helium bubbles under irradiation can embrittle the materials by weaken the grain boundary [38]. Additionally, the helium bubbles in matrix can act as obstacles to the free movement of dislocations, resulting in the hardening/embrittlement of materials [39,40].

3.4. PAS analysis

In order to further reveal the relation between the atomic level microstructure and the irradiation resistance properties of $Ti_2ZrHfV_{0.5}Mo_{0.2}$ HEA, the inherent defects within the $Ti_2ZrHfV_{0.5}Mo_{0.2}$ HEA and a representative traditional alloy (316L steel) were investigated using the technique of positron annihilation spectroscopy (PAS). The results of the PAS measurements were shown in Fig. 3(b). It is clear that the mount of equilibrium vacancy defects in $Ti_2ZrHfV_{0.5}Mo_{0.2}$ HEA is much higher than that in the 316L steel. Moreover, these vacancy defects distributed rather uniform from the depth of ~400 nm to the deeper bulk. The highly concentrated inherent vacancy defects in $Ti_2ZrHfV_{0.5}Mo_{0.2}$ HEA can effectively capture the implanted helium atoms, reduce the distortion around the vacancy defects and thus the lattice constant. This is consistent well with the result obtained by XRD.

Recently, Wang et al. theoretically evidenced that the equilibrium vacancy concentrations of HEAs are larger than that in pure metals and simple binary alloys [41]. Hence, it seems that the high vacancy concentration is a characteristic of high entropy alloy. In order to help readers better understand the irradiation resistant mechanism of high entropy alloy, a schematic diagram of the He ion being captured in the vacancy of atomic lattice is shown in Fig. 4.

In this study, the original existed high concentration of vacancy defects in $Ti_2ZrHfV_{0.5}Mo_{0.2}$ HEA can effectively capture the helium atoms, limiting thus the formation of intergranular helium bubbles and restraining the irradiation induced embrittlement of the $Ti_2ZrHfV_{0.5}Mo_{0.2}$ HEA. Moreover, the formation of small amount of helium bubbles in matrix, will greatly reduce the irradiation hardening of the $Ti_2ZrHfV_{0.5}Mo_{0.2}$ HEA. This can well explain the phenomenon of almost non hardening of irradiated $Ti_2ZrHfV_{0.5}Mo_{0.2}$ HEA (Fig. 3(a)). Similar to the metal oxide in ODS steels where the introduced interface between oxide particles and matrix can play as sink for helium atoms, the high concentration vacancy defects in $Ti_2ZrHfV_{0.5}Mo_{0.2}$ HEA can play the same role, improving thus the irradiation tolerance of material.

4. Conclusions

To summarize, we designed and prepared single BCC $Ti_2ZrHfV_{0.5}Mo_{0.2}$ HEA and did helium irradiation tests. The experimental results show that $Ti_2ZrHfV_{0.5}Mo_{0.2}$ HEA has excellent irradiation resistance and display very different properties from traditional alloys, the conclusions are as follows:

(1) The XRD diffraction peaks of traditional alloys usually shifts to the left and the lattice constant increases after irradiation, but The $Ti_2ZrHfV_{0.5}Mo_{0.2}$ HEA shifts to the right and the lattice constant decreases after irradiation. To our knowledge, this is for the first to report the abnormal XRD phenomenon of metallic alloys after irradiation.
(2) The nano-indentation test showed that the $Ti_2ZrHfV_{0.5}Mo_{0.2}$ HEA is almost no hardening after irradiation, which is obviously different from conventional alloys.
(3) The number density of helium bubble in all the irradiated samples was estimated to be around $(3.4–11.9)\times10^{21}$ m^{-3}. This

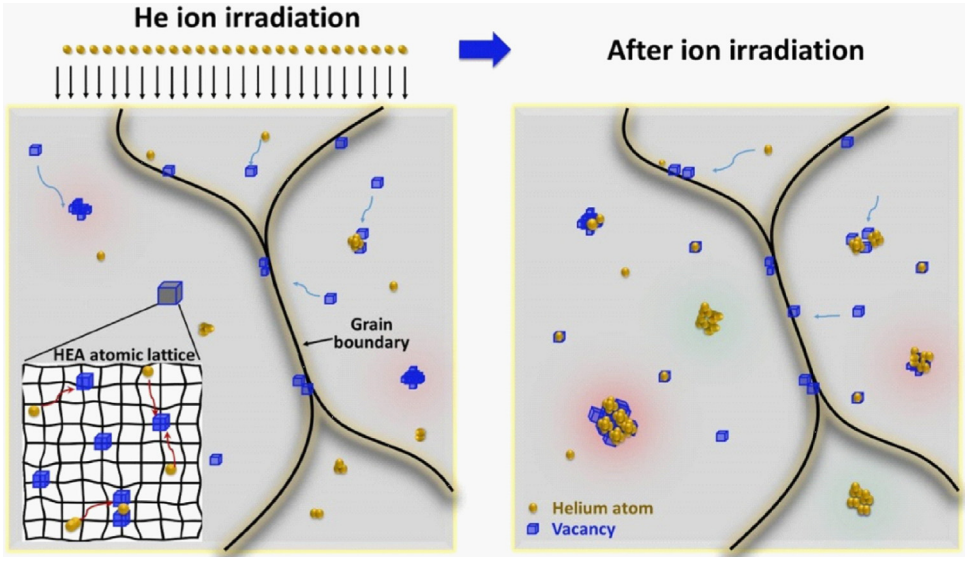

Fig. 4. A schematic diagram of the He ion being captured in the vacancy defects of $Ti_2ZrHfV_{0.5}Mo_{0.2}$ HEA.

value is much lower than the previous results for traditional alloys irradiated on the same condition.

(4) Positron annihilation experiments have found that $Ti_2ZrHfV_{0.5}Mo_{0.2}$ HEA has significantly higher vacancy concentration than conventional alloys, and the effect of these vacancies are similar to the oxide in ODS steel, which renders HEA high radiation resistance.

Acknowledgements

This work was supported by the National Natural Science Foundation of China (Nos. 11605271, 51471044, 51525401, 51771201 and 51401208), Youth Innovation Promotion Association, Chinese Academy of Sciences (No. 2016239), Dalian Support Plan for Innovation of High-level Talents (Top and Leading Talents, 2015R013), and Dalian Support Plan for Innovation of High-level Talents (Youth Technology Stars, 2016RQ005).

Appendix A. Supplementary data

Supplementary material related to this article can be found, in the online version, at doi:https://doi.org/10.1016/j.jmst.2018.09.034.

References

[1] S.J. Zinkle, G.S. Was, Acta Mater. 61 (2013) 735–758.
[2] H.P. Wang, S.J. Yang, L. Hu, B. Wei, Chem. Phys. Lett. 653 (1) (2016) 112–116.
[3] P. Lv, H.P. Wang, P.F. Zou, K. Zhou, L. Hu, B. Wei,J. Appl. Phys. 124 (2018), 025103.
[4] T.R. Allen, Y. Chen, X. Ren, K. Sridhara, L. Tan, G.S. Was, E. West, D.A. Guzonas, Comprehensive Nuclear Materials, Elsevier, 2012.
[5] R.M. Boothby, J. Nucl. Mater. 230 (1996) 148–157.
[6] A.F. Rowcliffe, L.K. Mansur, D.T. Hoelzer, R.K. Nanstad, J. Nucl. Mater. 392 (2009) 341–352.
[7] S.J. Zinkle, K.A. Terrani, L.L. Snead, Curr. Opin. Solid. State Mater. 20 (2016) 401–410.
[8] R.L. Klueh, J.P. Shingledecker, R.W. Swindeman, D.T. Hoelzer, J. Nucl. Mater. 341 (2005) 103–114.
[9] D.A. McClintock, M.A. Sokolov, D.T. Hoelzer, R.K. Nanstad, J. Nucl. Mater. 292 (2009) 353–359.
[10] M.K. Miller, D.T. Hoelzer, J. Nucl. Mater. 418 (2011) 307–310.
[11] G.R. Odette, M.J. Alinger, B.D. Wirth, Annu. Rev. Mater. Res. 38 (2008) 471–503.
[12] I.J. Beyerlein, A. Caro, M.J. Demkowicz, N.A. Mara, A. Misra, B.P. Uberuaga, Mater. Today. 16 (11) (2013) 443–449.
[13] Y. Zhang, M. Ishimaru, T. Varga, T. Oda, C. Hardiman, H. Xue, Y. Katoh, S. Shannon, W.J. Weber, Phys. Chem. Chem. Phys. 14 (2012) 13429–13436.
[14] H. Van Swygenhoven, P.M. Derlet, A.G. Froseth, Nat. Mater. 3 (2004) 399–403.
[15] E.M. Bringa, J.D. Monk, A. Caro, A. Misra, L. Zepeda-Ruiz, M. Duchaineau, F. Abraham, M. Nastasi, S.T. Picraux, Y.Q. Wang, D. Farkas, Nano Lett. 12 (2012) 3351–3355.
[16] F. Granberg, K. Nordlund, Mohammad W. Ullah, K. Jin, C. Lu, H. Bei, L.M. Wang, F. Djurabekova, W.J. Weber, Y. Zhang,Phys. Rev. Lett. 116 (2016), 135504.
[17] J.W. Yeh, S.K. Chen, S.J. Lim, J.Y. Gan, T.S. Chin, T.T. Shun, C.H. Tsau, S.Y. Chang, Adv. Eng. Mater. 6 (2004) 299–303.
[18] B. Cantor, I.T.H. Chang, P. Knight, A.J.B. Vincent, Mater. Sci. Eng. A 375–377 (2004) 213–218.
[19] M.C. Gao, J.W. Yeh, P.K. Liaw, Y. Zhang, High-Entropy Alloys: Fundamentals and Applications, Springer, 2016.
[20] B. Gludovatz, A. Hohenwarter, D. Catoor, E.H. Chang, E.P. George, R.O. Ritchie, Science 345 (2014) 1153–1158.
[21] Z. Li, K.G. Pradeep, Y. Deng, D. Raabe, C.C. Tasan, Nature 534 (2016) 227–230.
[22] C.Y. Lu, L.L. Niu, N.J. Chen, K. Jin, T.N. Yang, P.Y. Xiu, Y.W. Zhang, F. Gao, H.B. Bei, S. Shi, Mo-Rigen He, Ian M. Robertson, W.J. Weber, L.M. Wang, Nat. Commun. 7 (2016) 13564.
[23] N.A.P. Kiran Kumar, C. Li, K.J. Leonard, H. Bei, S.J. Zinkle, Acta Mater. 113 (2016) 230–244.
[24] Y.W. Zhang, G. Malcolm Stocks, K. Jin, C.Y. Lu, H.B. Bei, Brian C. Sales, L.M. Wang, L.K. Beland, R.E. Stoller, G.D. Samolyuk, M. Caro, A. Caro, W.J. Weber, Nat. Commun. 6 (2015) 8736.
[25] L. Yang, H. Ge, J. Zhang, T. Xiong, Q. Jin, Y. Zhou, X. Shao, B. Zhang, Z. Zhu, S. Zheng, X. Ma, J. Mater. Sci. Technol. 35 (2019), in press.
[26] S.Q. Xia, Z. Wang, T.F. Yang, Y. Zhang, J. Iron Steel Res. Int. 22 (2015) 879–884.
[27] S. Guo, C. Ng, J. Lu, C.T. Liu, J. Appl. Phys. 109 (2011) 103505.
[28] Y. Dong, K.Y. Zhou, Y.P. Lu, X.X. Gao, T.M. Wang, T.J. Li, Mater. Des. 57 (2014) 67–72.
[29] J.F. Ziegler, J.P. Biersack, U. Littmark, The Stopping and Range of Ions in Matter, Pergamon Press, 1985.
[30] R.E. Stoller, M.B. Toloczko, G.S. Was, A.G. Certain, S. Dwaraknath, F.A. Garner, Nucl. Instrum. Methods B 310 (2013) 75–80.
[31] W.C. Olivier, G.M. Pharr, J. Mater. Res. 7 (1992) 1564–1583.
[32] X.Z. Cao, P. Zhang, Q. Xu, K. Sato, G.D. Cheng, H.B. Wu, X.P. Jiang, R.S. Yu, B.Y. Wang,J. Phys. Conf. Ser. 443 (2013), 012017.
[33] Q.S. Cao, X. Ju, L.P. Guo, B.Y. Wang, Fusion Eng. Des. 89 (2014) 1101–1106.
[34] P. Hosemann, D. Frazer, M. Fratoni, A. Bolind, M.F. Ashby, Scr. Mater. 143 (2018) 181–187.
[35] P. Yvon, F. Carré, J. Nucl. Mater. 385 (2) (2009) 217–222.
[36] H.F. Huang, W. Zhang, M. De Los Reyes, X.L. Zhou, C. Yang, R. Xie, X.T. Zhou, P. Huai, H.J. Xu, Mater. Des. 90 (2016) 359–363.
[37] S.J. Zinkle, J.T. Busby, Mater. Today 12 (2009) 12–19.
[38] H. Trinkaus, B.N. Singh, J. Nucl. Mater. 323 (2003) 229–242.
[39] E.H. Lee, T.S. Byun, J.D. Hunn, K. Farrell, L.K. Mansur, J. Nucl. Mater. 296 (2001) 183–191.
[40] X.L. Zhou, H.F. Huang, R. Xie, G.J. Thorogood, C. Yang, Z.J. Li, H.J. Xu, J. Nucl. Mater. 467 (2015) 848–854.
[41] Z.J. Wang, C.T. Liu, P. Dou,Phys. Rev. Mater. 1 (2017), 043601.